

Experimental investigation of sinterability of PVA-coated Magnesium powders via mechanical milling using Electric Field-Assisted Sintering Technique

Yasemin Yahşi^{1,2*}, Sabriye Yuşan³, Sinan Akgöl⁴, Rasim İpek²

¹Dokuz Eylül University, Bergama Vocational School, Heavy Equipment Operator Program, Izmir, Turkey

²Ege University, Faculty of Engineering, Department of Mechanical Engineering, Izmir, Turkey

³Institute of Nuclear Sciences, Department of Nuclear Technology, Izmir, Turkey

⁴Ege University, Faculty of Science, Department of Biochemistry, Izmir, Turkey

Received 23 December 2023, received in revised form 5 July 2024, accepted 16 August 2024

Abstract

In this study, the sinterability of mechanically milled (MM) and Polyvinyl Alcohol (PVA) coated magnesium (Mg) powders is experimentally investigated using the Electric Field-Assisted Sintering Technique (FAST).

Active metals' surfaces are prone to atmospheric contamination, making preserving Mg powder surfaces critical for sintering processes. This study experimentally investigates the protective effectiveness of PVA coating on the surfaces of Mg powder. Particles derived from the addition of PVA to Mg powders during the MM process undergo scrutiny through Fourier-Transform-Infrared Spectroscopy (FT-IR), X-ray Diffraction (XRD), Energy Dispersive X-ray Spectroscopy (EDS) analysis, Scanning Electron Microscopy (SEM) imaging methods.

It has been observed that sintered samples of PVA-coated particles exhibit higher density and compression strength compared to non-coated samples. A sample milled for 30 min with 10 % PVA content achieves 99 % density and 195 MPa compression strength. This finding indicates that PVA coating enhances mechanical properties during sintering by promoting metal-metal contact.

Key words: mechanical milling (MM), PVA (Polyvinyl alcohol) coating, magnesium, Electric Field-Assisted Sintering Technique (FAST)

1. Introduction

Magnesium (Mg) is a widely used structural material with a density of 1.738 g cm^{-3} [1, 2]. Mg exhibits characteristics such as low density, high specific strength, hardness, damping, and biocompatibility [3]. Therefore, Mg and its alloys have garnered significant attention worldwide and have found extensive applications in the fields of aviation, military [4], automotive, computer, communication, consumer electronics, biomedical [5], and energy sectors [6, 7].

However, the closed-packed hexagonal (HCP) structure of Mg limits its formability [8]. For such materials, the powder metallurgy production method is recommended [9]. Additionally, powder metallurgy allows for the enhancement of various properties of

metallic materials, primarily mechanical characteristics [10].

Mechanical milling (MM) is commonly used as the powder preparation process for powder metallurgy. MM involves solid-state powder processing in a high-energy ball mill, which includes the repeated welding, fracturing, and rewelding of powder particles. Through MM, the microstructures of metallic powders are refined to fine grain sizes, and the powders undergo plastic deformation [11].

In this case, the material can achieve very high mechanical values depending on its plastic deformation sensitivity. However, during MM, the surfaces of reactive metals such as Mg are prone to rapid and easy physical and chemical contamination due to atmospheric effects [12]. During MM, the surfaces of

*Corresponding author: e-mail address: yasemin.yahsi@deu.edu.tr

metal powders, especially those prone to oxidation like Mg, become more mechanically active. Due to these reasons, the protection and storage of the surfaces of Mg powders from physical and chemical contamination are crucial for milling and sintering processes. For instance, it is desirable to have no oxide and other surface impurities during the sintering process that would hinder metal-to-metal contact between metallic powders. Sintering occurs more rapidly between clean surfaces. In such cases, high temperatures and long sintering times may not be necessary, and as a result, the benefits of mechanical milling, such as reduced grain size, crystal structure distortions, amorphization, and increased surface energy, can be preserved to the extent that sintering occurs at lower temperatures and shorter durations. On the other hand, preventing surface contamination of metallic powders during MM is a challenging and costly process compared to today's techniques.

During MM, impact forces induce particle deformation and fracture, creating new, clean, and more active metal surfaces. When these clean surfaces come into contact, they weld more easily. However, due to the higher susceptibility of mechanically active surfaces to contamination, milling is generally conducted in an inert gas or vacuum environment [11]. Despite the high equipment and operating costs associated with these measures, they may not always be as effective as desired. The surfaces of metal powders, such as Mg, need to be protected not only during the preparation for sintering but also during storage against atmospheric effects. Therefore, various coating methods are being developed to preserve the powders of active metals, especially Mg.

The coating of Mg in terms of mechanical, physical, chemical, and biological aspects has been investigated through various studies [13]. For instance, Mg has been physically coated using technologies such as magnetron sputtering [14], laser coating [15], electron beam [16], and ion implantation [17]. It has been mechanically coated through ball milling [18] and friction [19] or wear [20]. Chemical coatings have been applied through electro-deposition [21], sol-gel [22], electroless plating [23], micro-arc oxidation (MAO) [24], or plasma electrolytic oxidation (PEO).

Various metallic, ceramic, inorganic, organic, and polymeric materials have been employed in Mg coating processes [25, 26]. Aluminum (Al) [27], nickel (Ni) [28], titanium (Ti) [29], and tantalum (Ta) [30, 31] are the primary components used in metallic coatings. Ceramic and inorganic coatings consist of oxides such as TiO₂ [32], ZrO₂ [33, 34], SiO₂, CeO₂ [35], and Al₂O₃ [36]), phosphates (Ca-P salts) [21] as well as silicates, layered double hydroxide (LDH) [37, 38], and montmorillonite [35]. Organic and polymeric coatings include dopamine [39], DNA [40], tannic acid [41], PLA [42] or PLGA [43, 44], chitosan [45, 46],

and others. Furthermore, various composite or hybrid coatings combine two or more distinct coatings on Mg alloys.

As evidenced by these studies, research on various polymer coatings and method developments to protect metallic surfaces from environmental pollutants has been increasingly ongoing in recent years. In general, polymer-based coating systems have demonstrated excellent performance in establishing an effective barrier against metal surface corrosion [47]. In this context, it has been considered that Polyvinyl Alcohol (PVA) could be utilized through MM processes to preserve the surfaces of Mg powders. Polyvinyl alcohol ([CH₂CH(OH)]_n) is a tasteless, odorless, biocompatible polymer used in various fields such as the cosmetic industry, pharmaceutical sector, printing, ceramics, steel, electronics, electroplating, and more. PVA and its composites are synthetic polymers with excellent chemical resistance and optical and physical properties. PVA is increasingly used as a packaging and coating material [48, 49].

The literature review indicates that traditional Mg/PVA composites have been produced using various methods. However, MM followed by FAST (Field-Assisted Sintering Technique) methods have not been employed to produce Mg/PVA composites. Therefore, instead of providing traditional Mg/PVA composites with a simple composition and uniform properties, biodegradable Mg/PVA materials have been investigated.

Mg is essential for the human body and is crucial in numerous biological processes. Mg and Mg alloys can be utilized in medical implants, bone screws, plates, and other surgical equipment [50, 51]. However, it is essential to understand how these materials behave when they come into contact with bodily fluids or tissues in such applications. In vitro corrosion tests have been conducted to evaluate the biological durability of these materials in biological environments.

In this study, the feasibility of coating Mg powders with PVA during MM has been experimentally investigated, and the effectiveness of this coating in protecting the Mg powder surfaces from potential atmospheric effects has been examined. Additionally, the impact of milling duration and the quantity of PVA on the compression strength and density values of samples sintered with FAST has been evaluated. Furthermore, corrosion resistance in the SBF environment has also been measured.

2. Experimental

2.1. Material

Magnesium (Mg) powders used in this study were sourced from Kumas Manyezit Sanayi A.S. (Kütahya,

Türkiye) with a purity level of $\geq 99.3\%$ and a particle size of $\leq 220\ \mu\text{m}$. Polyvinyl Alcohol (PVA) in powder form, with the chemical formula $(\text{CH}_2\text{CHOH})_n$, was obtained from the ZAG Kimya brand, featuring a density of $0.4\text{--}0.6\ \text{g cm}^{-3}$ and a purity of 88.8% . The PVA raw powder had a molecular weight (M_w) of $84,000\text{--}89,000\ \text{g mol}^{-1}$ and was procured from ZAG Kimya.

2.2. Preparation of powder samples

Mg powders underwent high-energy ball milling using stainless steel balls with a diameter of 10 mm and a stainless steel milling container. The milling containers were treated in a glovebox under an argon-protective atmosphere. The ball-to-powder ratio was maintained at 20:1, and ball milling was conducted at a speed of 160 rpm.

Understanding the MM process requires an accurate definition of the dynamics underlying the formation of stresses within the particles [11, 52, 53, 54]. For this purpose, the milling performed at different times must be considered. In this study, MM was conducted for two different durations: 30 min (Mg_{30}) and 60 min (Mg_{60}).

Mg powders subjected to MM for 30 and 60 min had PVA powder added during the final 10 min of the milling process. Along with the PVA powder, a flexible binder, boric acid, was used at 10 % of the PVA amount. The addition process occurred in an argon atmosphere through a valve in the milling containers. The temperature of the container was approximately 90°C when the PVA was added. PVA was added to different milling containers at concentrations of 10 and 20 % by weight of Mg (30 min of milling with 10 % PVA added to Mg: $\text{Mg}_{30}\text{PVA}10$; 30 min of milling with 20 % PVA added to Mg: $\text{Mg}_{30}\text{PVA}20$; 60 min of milling with 10 % PVA added to Mg: $\text{Mg}_{60}\text{PVA}10$; 60 min of milling with 20 % PVA added to Mg: $\text{Mg}_{60}\text{PVA}20$).

$\text{Mg}_{30}\text{PVA}10$ was mixed with 1 g of powder in 30 ml of ethyl alcohol for 2 h using a magnetic stirrer, aiming to remove the PVA from its surface. Subsequently, it was filtered through filter paper to remove ethyl alcohol. The powders were then dried in a protective argon atmosphere ($\text{Mg}_{30}\text{PVA}10$ powders whose surface had been cleared of PVA with ethyl alcohol: Mg_a).

2.3. Preparation of sintered samples

The sintering process occurred in a graphite mold with a height of 50 mm. Two punches, each with a diameter of 20 mm, were utilized. As a result, cylindrical samples with a diameter of 20 mm and a height of 10 mm were obtained. Mg, Mg_{30} , Mg_{60} , $\text{Mg}_{30}\text{PVA}10$, and $\text{Mg}_{60}\text{PVA}20$, Mg_a particles were sintered under uniaxial and double-action press at 45 MPa pressure at 400°C for 5 min. All processes were carried out in

the argon atmosphere. The electrically assisted sintering device is a laboratory-scale equipment manufactured by Tugem.

Pure magnesium (Mg) has low corrosion resistance. Only Mg_a powders do not have a coating such as PVA or MgO on their surfaces, which caused catastrophic corrosion behavior when sintered Mg_a samples were exposed to SBF. A specific heat treatment was applied exclusively to Mg_a samples to address this. This specific procedure was necessary only for Mg_a samples due to their lack of surface coating and inherent low corrosion resistance. Mg_a sintered samples, tested in vitro, were sintered at 400°C for 5 min, then the temperature was reduced to 100°C , the argon atmosphere was removed, and sintering continued for another 20 min. This additional step aimed to create a corrosion-resistant oxide layer around the sintered sample, enhancing its stability and corrosion resistance.

2.4. Density measurement

The Archimedes method was used at room temperature to measure the actual density of the samples. Each sample was separately measured five times. The sample's relative density was determined by dividing the actual density by the theoretical density. Kern ABS 220-4M was used for measurements.

The theoretical densities of samples were calculated with Eq. (1):

$$\frac{1}{\rho_t} = w_{\text{Mg}} \frac{1}{\rho_{\text{Mg}}} + w_{\text{PVA}} \frac{1}{\rho_{\text{PVA}}}, \quad (1)$$

where ρ_t is the theoretical density of the FAST'ed sample, ρ_{Mg} and ρ_{PVA} are the densities of Mg and PVA ($\rho_{\text{Mg}} = 1.74\ \text{g cm}^{-3}$, $\rho_{\text{PVA}} = 1.16\ \text{g cm}^{-3}$), and w_{Mg} and w_{PVA} are the weight fractions of Mg and PVA in the sample, respectively.

2.5. FT-IR and XRD analysis

Fourier Transform Infrared Spectroscopy (FTIR) was used to characterize the presence of some chemical groups of PVA on the powder surface. FT-IR measurements were conducted using a Perkin Elmer Spectrum 100 instrument. The XRD analysis of the PVA, Mg, and $\text{Mg}_{30}\text{PVA}10$ samples was carried out using the PANalytical, Empyrean Model with K_α Cu radiation ($\lambda = 1.54\ \text{\AA}$), covering a diffraction angle range of 5° to 85° (ICSD reference codes: 98-007-6748, 92-020-3213, 98-017-0905).

2.6. Microstructural and mechanical properties

Scanning Electron Microscope (SEM) images were acquired using the Thermo Scientific Apreo S instru-

Table 1. The chemical composition of SBF solution [55]

Chemical type	NaCl	CaCl ₂	KCl	KH ₂ PO ₄	MgSO ₄ · 7H ₂ O	NaHCO ₃	Na ₂ HPO ₄	C ₆ H ₁₂ O ₆
Chemical amount (g L ⁻¹)	8.000	0.185	0.400	0.060	0.100	0.350	0.480	1.000

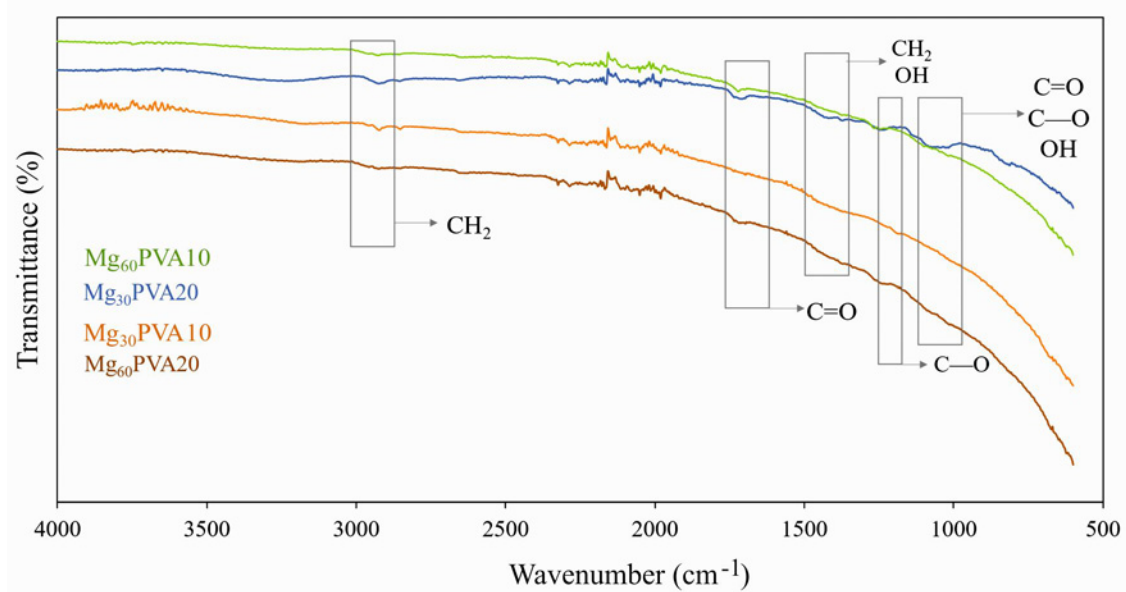


Fig. 1. The FT-IR spectrum of Mg particles with added PVA during the last 10 min of the MM process.

ment (Detectors: ETD, EDS; Sample chamber inner diameter: 340 mm; Electron gun: Schottky FEG gun) and Carl Zeiss 300VP SEM device. The specimens were coated with gold/palladium (Au/Pd) using the Leica EM ACE600 coating device for SEM imaging of non-conductive samples. Compression strength tests were conducted using a Shimadzu (AG-IS 100 kN) tensile-compression tester at a constant speed of 0.2 mm min⁻¹.

2.7. Investigation of corrosion behavior

Corrosion tests were conducted in simulated body fluid (SBF) with a pH of 7.4 at a temperature of 36 ± 1.5 °C. The SBF solution was prepared according to Kokubo's method [55], and its chemical composition is shown in Table 1.

The corrosion behavior of the samples (FAST'ed; Mg₃₀, Mg₃₀PVA10, Mg_a) in SBF was investigated using immersion experiments. These tests were employed to determine sample weight loss and pH changes during degradation. Three distinct measurements were performed for each sample, and the average values were reported. The pH of the solution was measured using a pH meter (Hanna HI2002-02). The weight loss was calculated using Eq. (2):

$$\text{Weight loss} = W_i - W_t, \quad (2)$$

where W_i is the initial weight and W_t is the dry weight at time t .

3. Results and discussion

3.1. FT-IR analysis

The FT-IR spectrum of Mg particles with added PVA in the last 10 min of the MM process is presented in Fig. 1.

The % transmittance spectrum of the coated Mg powders is depicted in Fig. 1. For PVA, the characteristic absorption peaks are observed at 2936 cm⁻¹ (asymmetric stretching of CH₂), 2906 cm⁻¹ (symmetric stretching of CH₂), 1643 cm⁻¹ (due to water absorption), 1416 cm⁻¹ (CH₂ bending), 1325 cm⁻¹ (δ (OH), rocking with CH wagging), 1138 cm⁻¹ (shoulder stretching of C—O) (crystalline sequence of PVA), 1083 cm⁻¹ (stretching of C—O and bending of OH) (amorphous sequence of PVA), 916 cm⁻¹ (CH₂ rocking), 822 cm⁻¹ (C—C stretching) [56, 57].

The FT-IR analysis of Mg particles with added PVA in the final 10 min of MM revealed peaks resembling those found in pure PVA. This suggests that PVA remained largely unchanged during the MM coating process.

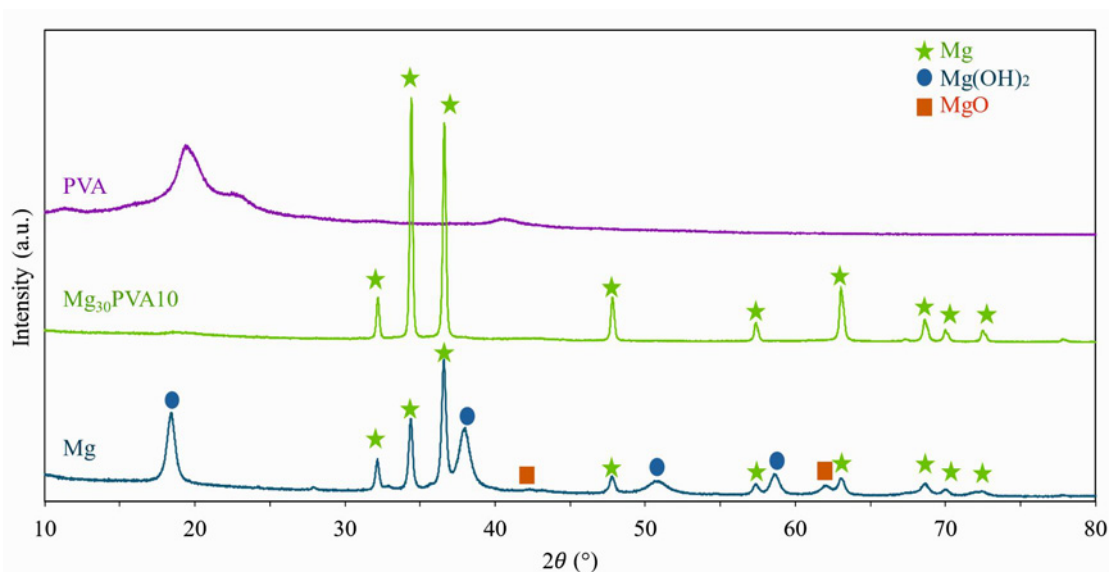


Fig. 2. XRD patterns of the PVA, Mg, and Mg₃₀PVA10 powders.

3.2. XRD analysis

The XRD analysis of PVA, Mg, and Mg₃₀PVA10 is given in Fig. 2.

As reported in the literature, the XRD pattern of PVA displayed characteristic peaks corresponding to PVA [58]. The uncoated Mg sample exhibited characteristic peaks corresponding to magnesium (Mg), magnesium oxide (MgO), and magnesium hydroxide (Mg(OH)₂) compounds [59, 60]. The Mg₃₀PVA10 sample also displayed characteristic peaks corresponding to both PVA and Mg. Upon examination of the XRD peaks of Mg and Mg₃₀PVA10 samples, while Mg compounds (MgO, Mg(OH)₂) were clearly observed in the Mg sample, they were not detected in the Mg₃₀PVA10 sample. This suggests that the presence of PVA on the surface prevents the formation of Mg compounds.

3.3. SEM images and EDS analysis of powder samples

SEM images of Mg, Mg₃₀, Mg₆₀, Mg₃₀PVA10, Mg₃₀PVA20, Mg₆₀PVA10, and Mg₆₀PVA20 particles are presented in the Fig. 3a–g. The SEM images also include elemental distribution (carbon) maps of Mg₃₀PVA10, Mg₃₀PVA20, Mg₆₀PVA10, and Mg₆₀PVA20 particles.

SEM images illustrated that particles of Mg, Mg₃₀, and Mg₆₀ underwent plastic deformation, crushing, and fragmentation due to MM. In contrast, particles subjected to MM with added PVA exhibited clear evidence of PVA presence on the surface, which is evident in both SEM mapping images and the similarity in FT-IR graphs. The distribution of C atoms from PVA's structure onto the powder surface was dis-

tinctly observed in mapping images. During the EDS analysis, no elements other than those expected due to the nature of Mg and PVA were detected. The elemental distribution of carbon is shown to distinguish PVA. A homogeneous distribution is observed on the coated surfaces.

EDS analysis of the Mg_a is shown in Fig. 4. Measurements were taken from three different spots on the powders. The analysis revealed the presence of no elements other than Mg.

The absence of any element other than Mg when PVA is removed from Mg₃₀PVA10 powders with alcohol is highly significant. The absence of MgO on the surface indicates a successful prevention of Mg oxidation.

3.4. SEM images and EDS analysis of sintered samples

SEM images of Mg, Mg₃₀PVA10, and Mg_a FAST'ed samples are presented in the Figs. 5a–c. After the compression test, the fractured surfaces of Mg₃₀PVA10 and Mg₆₀PVA20 FAST'ed samples are shown in Figs. 5d,e.

As previously investigated [61], the “necking” mechanism, a hallmark of the classical sintering process, can be observed from the bonding between particles depicted in Fig. 5a in sintered Mg raw powders.

In the FAST'ed Mg₃₀PVA10 sample (Fig. 5b), the particles are stacked in the direction of layers, and their arrangement is more planar compared to the particles in the Mg_a sample (Fig. 5c). In the FAST'ed Mg_a sample, bending and shortening in plate-like particles are observed.

In samples containing PVA, it is observed after sintering that the majority of PVA has evaporated, while

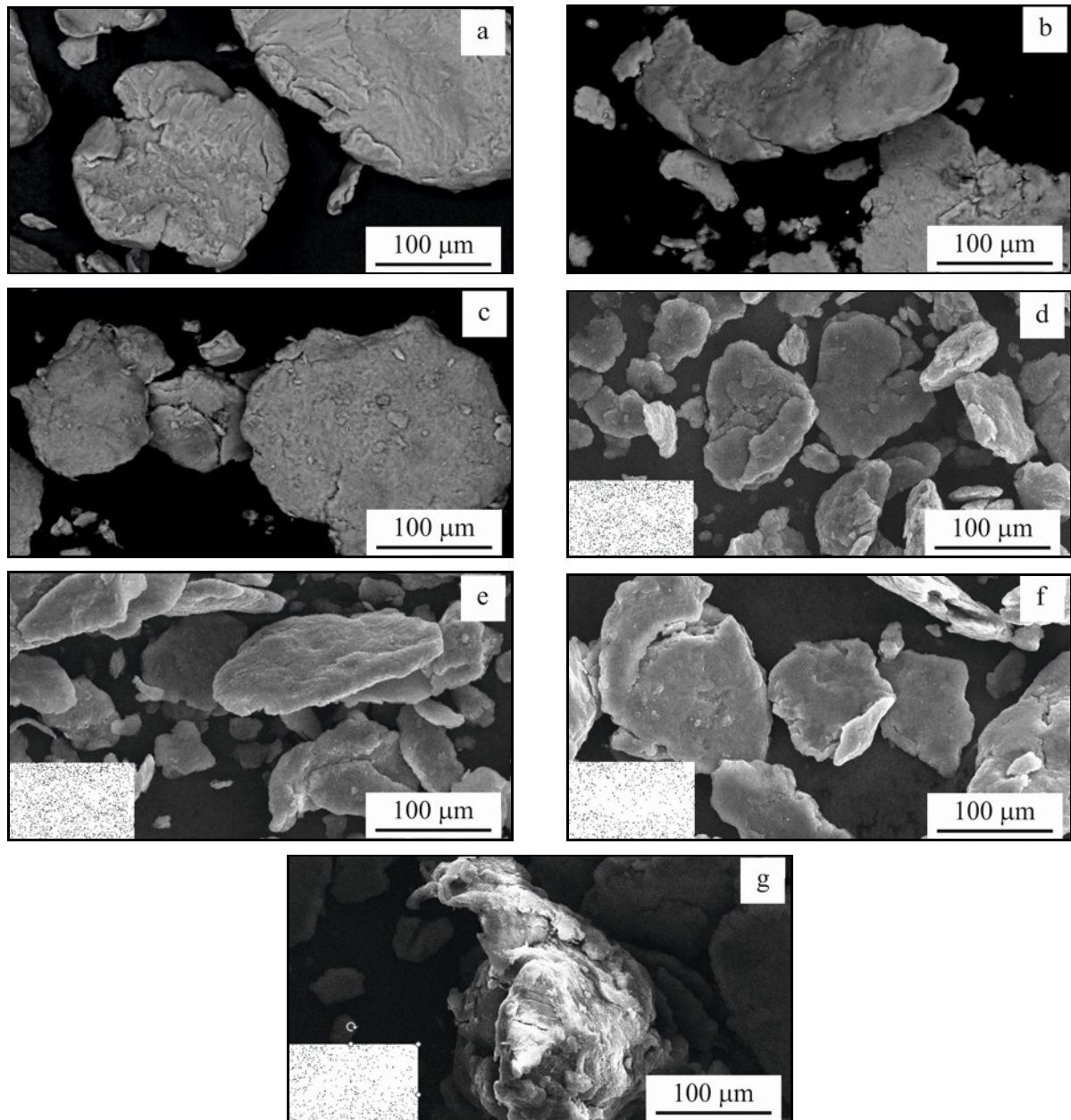


Fig. 3. SEM images and EDS analysis of the particles: (a) Mg, (b) Mg₃₀, (c) Mg₆₀, (d) Mg₃₀PVA10, (e) Mg₃₀PVA20, (f) Mg₆₀PVA10, and (g) Mg₆₀PVA20.

the remaining portion has accumulated in dark areas, leading to the formation of pores around them. EDS results indicate the presence of PVA residues (existence of carbon) in these dark areas.

FAST relies on short-circuiting from several points, leading to the generation of high voltages along the short-circuited path. This results in high temperatures in the surrounding areas. A significant amount of PVA initially evaporates due to the Joule heating (JH) effect. However, it is observed, albeit in small amounts, that PVA residues undergo degradation due to the high heat generated by the short-circuit current, leading to the formation of 'unbonding-pore-dark col-

ored areas' as indicated by EDS data (Figs. 5b,d,e). SEM data confirm the attainment of high density, with the proportion of residual PVA being quite low. Treatment with alcohol (Mg_a) results in samples with higher density, with almost no PVA residues being encountered.

3.5. Density and compressive strength

The compression strengths and density values of the sintered samples are illustrated in Fig. 6. Mg in Fig. 6 is a sintered sample from raw powders.

Examination of density and compression strength

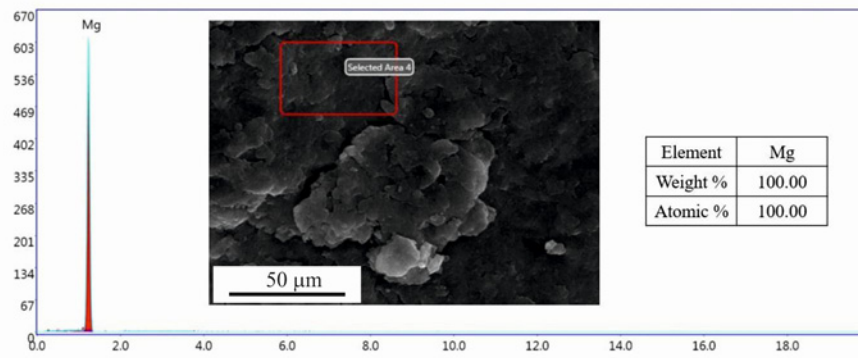


Fig. 4. The EDS analysis conducted on Mg₃₀PVA10 powders after treatment with alcohol (Mg_a).

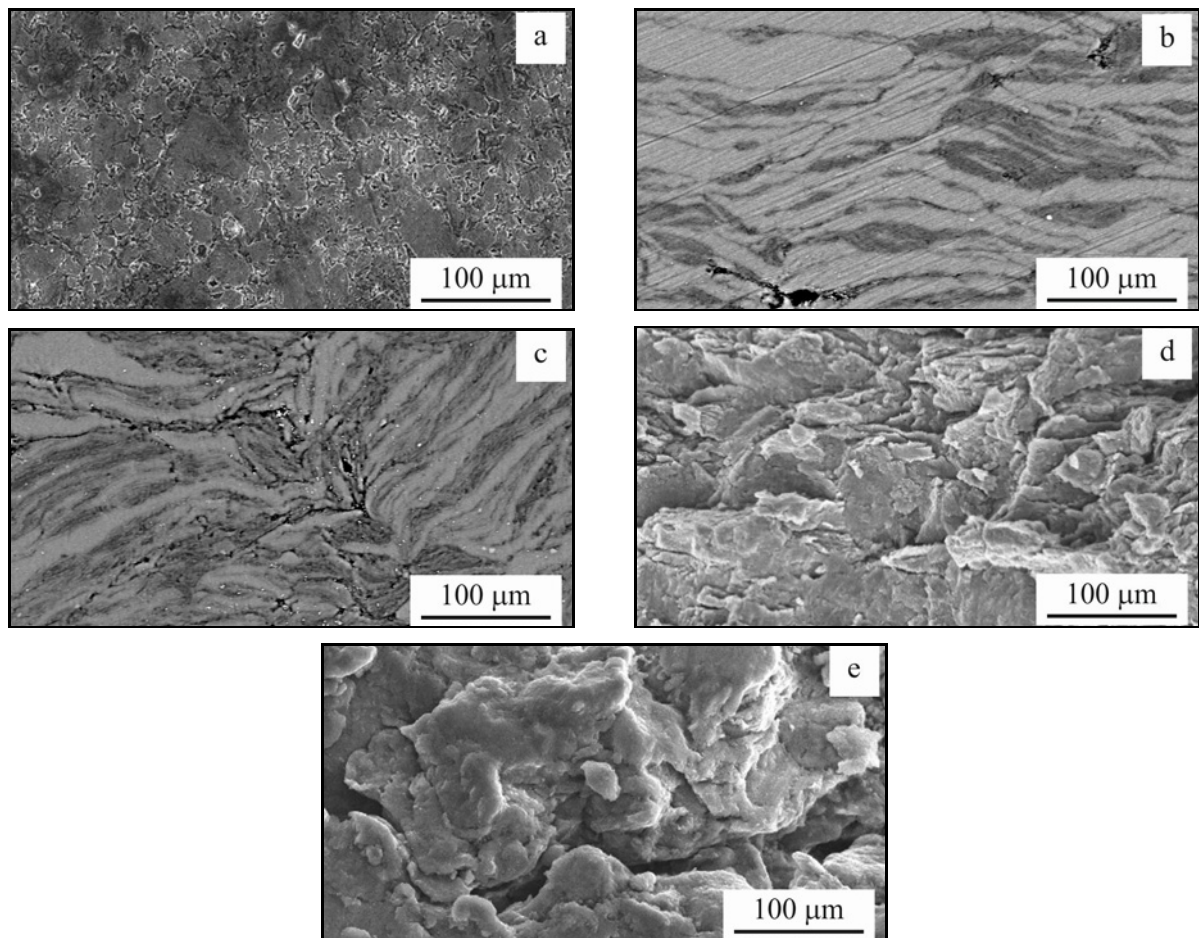


Fig. 5. SEM images of (a) Mg, (b) Mg₃₀PVA10, and (c) Mg_a FAST'ed samples; the fractured surfaces of (d) Mg₃₀PVA10 and (e) Mg₆₀PVA20 FAST'ed samples.

values for sintered samples revealed that samples sintered after MM exhibited higher density than sintered samples from raw Mg powders. Increasing MM time led to an increase in density and compression strength values. Fresh surfaces were created on the surface of Mg powders using the mechanical milling method. In this way, the contact between the particles is achieved through cleaner and fresher surfaces, which increases

the sintering efficiency and, consequently, the density and compressive strength.

The density and compression strength values of the samples obtained by sintering PVA-coated particles are higher than those without coating. The PVA coating applied on the particles moves away from the particle contact points with sintering temperatures and pressure, and contact with clean surfaces is en-

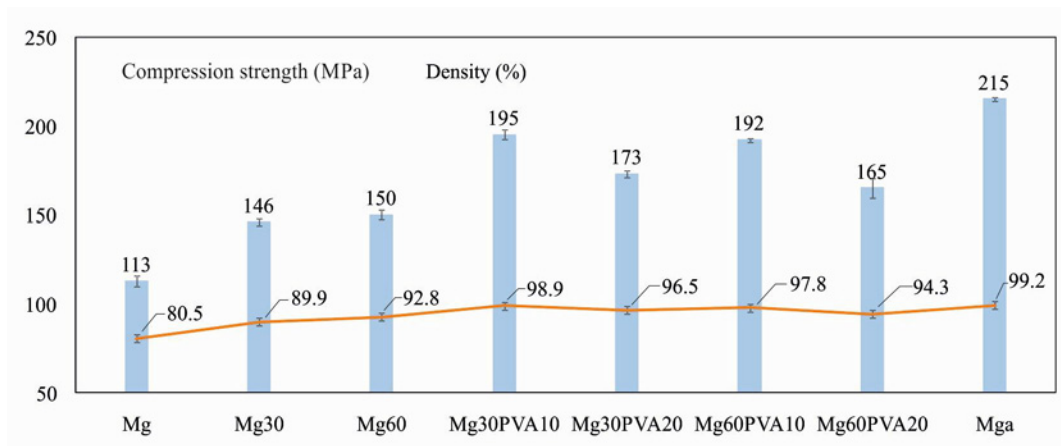


Fig. 6. Compression strengths and density values of the FAST'ed samples.

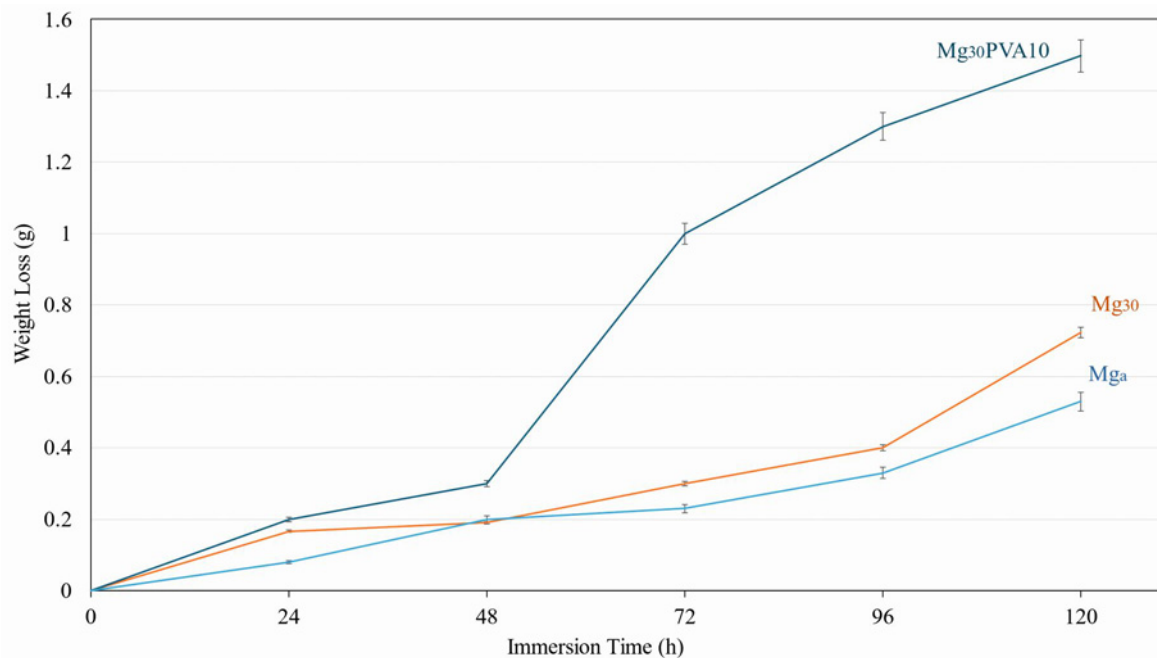


Fig. 7. Weight loss of samples after immersion in SBF for 120 h.

sured. This results in better bonding and higher density between particles. High density contributes to increased mechanical properties, especially compressive strength.

When examining the last 10 min of MM with added PVA quantities, a 10 % PVA quantity resulted in higher density and compression strength values compared to 20 % for both milling durations. An increase in the amount of PVA led to a decrease in compression strength and density values.

The high efficiency provided by the FAST technique results in more and stronger bonding points between particles. This technique improves mechanical properties by increasing the homogeneity and density of the microstructure. In this study, the maximum compression strength was obtained by sintering Mg

powders (Mg_a) whose surfaces were cleaned with alcohol to remove PVA. This was attributed to the effective sintering of the sample thanks to the fresh Mg contact points.

3.6. pH and weight loss determination

The weight loss and pH values of the Mg_{30} , $Mg_{30}PVA_{10}$, and Mg_a samples during immersion in simulated body fluid (SBF) for 120 h are shown in Figs. 7 and 8, respectively.

In this study, Mg_a exhibited the highest resistance to corrosion in the SBF environment. Although Mg_{30} ranks second in terms of corrosion resistance, the corrosion resistance of Mg_{30} and Mg_a is close to each other.

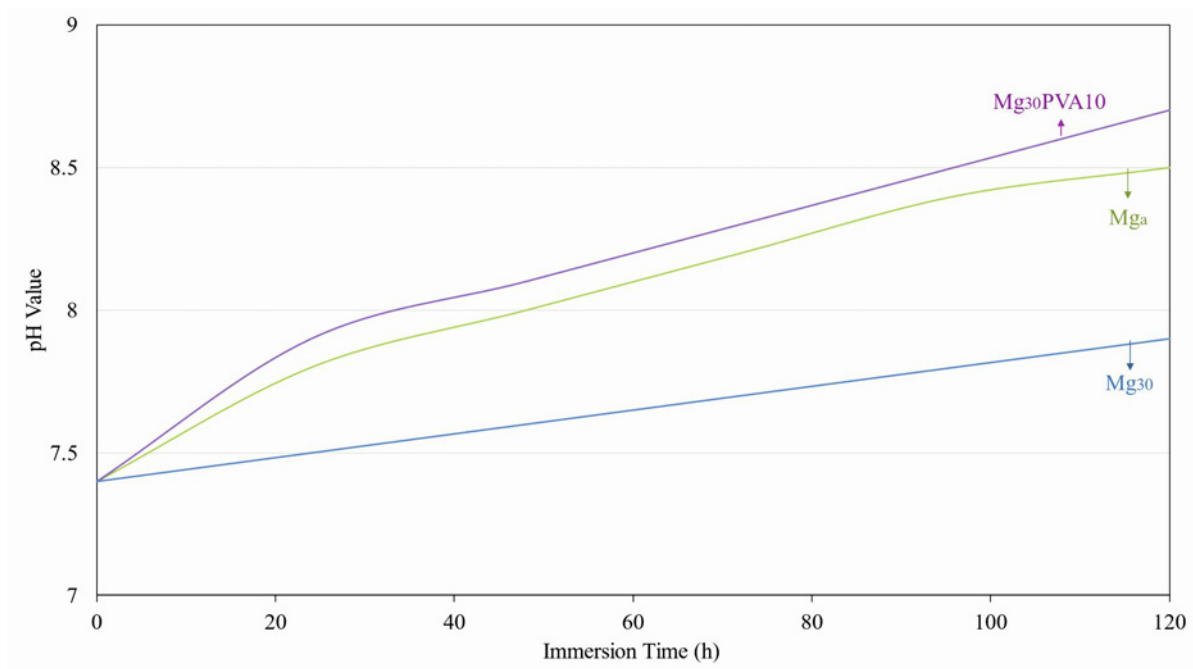


Fig. 8. pH values of samples after immersion in SBF for 120 h.

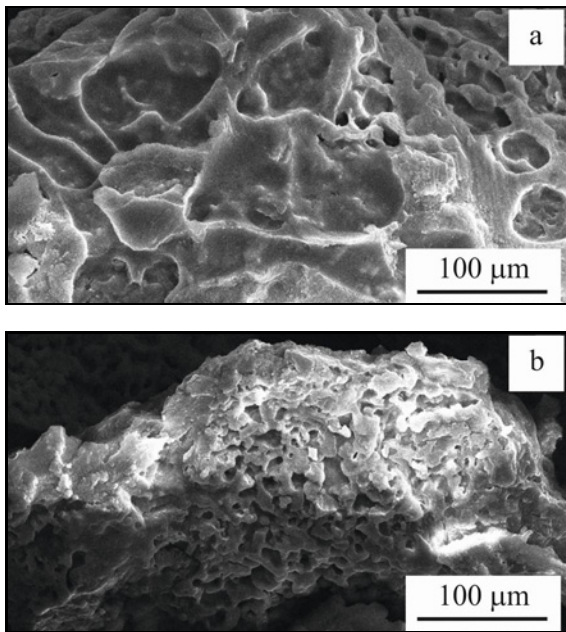


Fig. 9. SEM images of the FAST'ed samples after the corrosion tests: (a) Mg₃₀ and (b) Mg₃₀PVA10.

The most susceptible sample to corrosion in SBF was Mg₃₀PVA10. This susceptibility is believed to be due to the rapid dissolution of PVA on the surface in SBF, followed by a swift attack of the SBF solution on the fresh surface of Mg particles. It is thought that in other samples, due to the presence of an oxide layer on the surface, such a rapid attack did not occur, whereas in the Mg₃₀PVA10 sample, there was a rapid attack on pure Mg.

The least increase in pH was observed for Mg₃₀, followed by Mg_a. The highest increase was observed in the Mg₃₀PVA10 sample.

The SEM images in Figs. 9a,b were obtained after conducting corrosion tests in SBF solution on Mg₃₀ and Mg₃₀PVA10 FAST'ed samples.

FAST'ed Mg₃₀PVA10 exhibited the most severe corrosion damage. On the other hand, the FAST'ed Mg₃₀ sample emerged as the most corrosion-resistant among the other samples. The surface of both samples is covered with pits of varying depths. The formation of such pits in the SBF environment could aid in creating pores that may support cell adhesion in future in vitro implant studies.

4. Conclusions

The FT-IR analysis revealed that the characteristic absorption peaks of PVA were observed in the spectrum of Mg particles with added PVA, indicating that PVA remained largely chemically unchanged during the mechanical milling coating process.

XRD analysis indicated that the presence of PVA on the surface of Mg₃₀PVA10 prevented the formation of Mg compounds such as MgO and Mg(OH)₂.

SEM images and EDS analysis showed that particles subjected to mechanical milling with added PVA exhibited evidence of PVA presence on the surface. The distribution of carbon atoms from PVA onto the particles surface was distinctly observed.

SEM images and EDS analysis of Mg₃₀PVA10 particles after treatment with alcohol revealed the ab-

sence of any element other than Mg when PVA was removed, indicating successful prevention of Mg oxidation.

The addition of PVA as a coating protection substance, especially at a 10 % quantity during the final 10 min of milling, resulted in the highest density and compression strength values. Moreover, sintering alcohol-purified Mg powders led to the highest compression strength, highlighting the effectiveness of sintering non-oxide Mg surfaces.

After corrosion testing, SEM images of FAST'ed Mg30PVA10 samples showed the most severe corrosion damage, while FAST'ed Mg_a samples emerged as the most corrosion-resistant among the other samples. The presence of pits on the surface of both samples in the SBF environment suggests potential pore formation that may support cell adhesion in future in vitro implant studies.

Overall, experimental findings demonstrate that Mg particles can be coated with PVA using MM and the effectiveness of PVA coating in preventing Mg oxidation.

Acknowledgement

Part of this study was supported by the Ege University Scientific Research Fund (FOA-2021-22503).

References

- J. Tan and S. Ramakrishna, Applications of magnesium and its alloys: A review, *Applied Sciences* 11 (2021) 6861. <https://doi.org/10.3390/app11156861>
- S. Jayasathyakawin, M. Ravichandran, N. Baskar, C. A. Chairman, R. Balasundaram, Mechanical properties and applications of Magnesium alloy – Review, *Materials Today: Proceedings* 27 (2020) 909–913. <https://doi.org/10.1016/j.matpr.2020.01.255>
- N. R. Neelamegham, Primary production of magnesium, in *Fundamentals of Magnesium Alloy Metallurgy: A volume in Woodhead Publishing Series in Metals and Surface Engineering*, Elsevier Inc., 2013, pp. 1–32. <https://doi.org/10.1533/9780857097293.1>
- F. Czerwinski, Magnesium and Its Alloys. In: *Magnesium Injection Molding*. Springer, Boston, MA, 2008. https://doi.org/10.1007/978-0-387-72528-4_1
- X. Shen, Z. Zhang, C. Cheng, C. Liu, N. Ma, D. Sun, D. Li, C. Wang, Bone regeneration and antibacterial properties of calcium-phosphorus coatings induced by gentamicin-loaded polydopamine on magnesium alloys, *Biomedical Technology* 5 (2024) 87–101. <https://doi.org/10.1016/j.bmt.2023.06.002>
- I. Polmear, D. StJohn, J.-F. Nie, M. Qian, *Magnesium Alloys*, in *Light Alloys*, (fifth Edition), 2017, pp. 287–367. <https://doi.org/10.1016/B978-0-08-099431-4.00006-3>
- G. S. Frankel, Magnesium alloys: Ready for the road, *Nature Materials* 14 (2015) 1189–1190. <https://doi.org/10.1038/nmat4453>
- D. Sun, M. Ponga, K. Bhattacharya, M. Ortiz, Proliferation of twinning in hexagonal close-packed metals: Application to magnesium, *J. Mech. Phys. Solids* 112 (2017) 368–384. <https://doi.org/10.1016/j.jmps.2017.12.009>
- J. Alias, W. S. W. Harun, H. Mas Ayu, A review on the preparation of magnesium-based alloys prepared by powder metallurgy and the evolution of microstructure and mechanical properties, in *Key Engineering Materials*, Trans. Tech. Publications Ltd, 2019, pp. 3–10. <https://doi.org/10.4028/www.scientific.net/KEM.796.3>
- C. J. Bettles, Magnesium powder metallurgy: Process and materials opportunities, *Journal of Materials Engineering and Performance* 17 (2008) 297–301. <https://doi.org/10.1007/s11665-008-9201-0>
- C. Suryanarayana, Mechanical Alloying and Milling, *Progress in Materials Science* 46 (2001) 1–184. [https://doi.org/10.1016/S0079-6425\(99\)00010-9](https://doi.org/10.1016/S0079-6425(99)00010-9)
- J. E. Gray, B. Luan, Protective coatings on magnesium and its alloys – A critical review, *Journal of Alloys and Compounds* 336 (2002) 88–113. [https://doi.org/10.1016/S0925-8388\(01\)01899-0](https://doi.org/10.1016/S0925-8388(01)01899-0)
- Z. Z. Yin, W. C. Qi, R. C. Zeng, X. B. Chen, C. D. Gu, S. K. Guan, Y. F. Zheng, Advances in coatings on biodegradable magnesium alloys, *Journal of Magnesium and Alloys* 8 (2020) 42–65. <https://doi.org/10.1016/j.jma.2019.09.008>
- R. C. Zeng, K. Jiang, S. Q. Li, F. Zhang, H. Z. Cui, E. H. Han, Mechanical and corrosion properties of Al/Ti film on magnesium alloy AZ31B, *Front Mater. Sci.* 9 (2015) 66–76. <https://doi.org/10.1007/s11706-015-0272-1>
- Y. Guo, Y. Zhang, Z. Li, S. Wei, T. Zhang, L. Yang, S. Liu, Microstructure and properties of in-situ synthesized ZrC-Al3Zr reinforced composite coating on AZ91D magnesium alloy by laser cladding, *Surface and Coatings Technology* 334 (2018) 471–478. <https://doi.org/10.1016/j.surfcoat.2017.12.007>
- Y. Gao, C. Wang, H. Pang, H. Liu, M. Yao, Broad-beam laser cladding of Al-Cu alloy coating on AZ91HP magnesium alloy, *Applied Surface Science* 253 (2007) 4917–4922. <https://doi.org/10.1016/j.apsusc.2006.10.075>
- J. Liu, Y. Zheng, Y. Bi, Y. Li, Y. Zheng, Improved cytocompatibility of Mg-1Ca alloy modified by Zn ion implantation and deposition, *Materials Letters* 205 (2017) 87–89. <https://doi.org/10.1016/j.matlet.2017.06.055>
- M. Mhaede, F. Pastorek, B. Hadzima, Influence of shot peening on corrosion properties of biocompatible magnesium alloy AZ31 coated by dicalcium phosphate dihydrate (DCPD), *Materials Science and Engineering C* 39 (2014) 330–335. <https://doi.org/10.1016/j.msec.2014.03.023>
- Y. D. He, H. F. Fu, X. G. Li, W. Gao, Microstructure and properties of mechanical attrition enhanced electroless Ni-P plating on magnesium alloy, *Scripta Materialia* 58 (2008) 504–507. <https://doi.org/10.1016/j.scriptamat.2007.10.051>
- X. Xiong, Y. Yang, J. Li, M. Li, J. Peng, C. Wen, X. Peng, Research on the microstructure and properties of a multi-pass friction stir processed 6061Al coating for AZ31 Mg alloy, *Journal of Magnesium and Alloys*

- 7 (2019) 696–706.
<https://doi.org/10.1016/j.jma.2019.09.001>
- [21] H. Wang, S. Guan, Y. Wang, H. Liu, H. Wang, L. Wang, C. Ren, S. Zhu, K. Chen, In vivo degradation behavior of Ca-deficient hydroxyapatite coated Mg-Zn-Ca alloy for bone implant application, *Colloids and Surfaces B: Biointerfaces* 88 (2011) 254–259.
<https://doi.org/10.1016/j.colsurfb.2011.06.040>
- [22] J. H. Gao, X. Y. Shi, B. Yang, S. S. Hou, E. C. Meng, F. X. Guan, S. K. Guan, Fabrication and characterization of bioactive composite coatings on Mg-Zn-Ca alloy by MAO/sol-gel, *J. Mater. Sci. Mater. Med.* 22 (2011) 1681–1687.
<https://doi.org/10.1007/s10856-011-4349-9>
- [23] A. A. Zuleta, E. Correa, J. G. Castaño, F. Echeverría, A. Baron-Wiecheć, P. Skeldon, G. E. Thompson, Study of the formation of alkaline electroless Ni-P coating on magnesium and AZ31B magnesium alloy, *Surface and Coatings Technology* 321 (2017) 309–320.
<https://doi.org/10.1016/j.surfcoat.2017.04.059>
- [24] K. Dong, Y. Song, D. Shan, E. H. Han, Corrosion behavior of a self-sealing pore micro-arc oxidation film on AM60 magnesium alloy, *Corros. Sci.* 100 (2015) 275–283.
<https://doi.org/10.1016/j.corsci.2015.08.004>
- [25] Z. Z. Yin, W. C. Qi, R. C. Zeng, X. B. Chen, C. D. Gu, S. K. Guan, Y. F. Zheng, Advances in coatings on biodegradable magnesium alloys, *Journal of Magnesium and Alloys* 8 (2020) 42–65.
<https://doi.org/10.1016/j.jma.2019.09.008>
- [26] A. Saberi, H. R. Bakhsheshi-Rad, S. Abazari, A. F. Ismail, S. Sharif, S. Ramakrishna, M. Daroonparvar, F. Berto, A comprehensive review on surface modifications of biodegradable magnesium-based implant alloy: Polymer coatings opportunities and challenges, *Coatings* 11 (2021) 747.
<https://doi.org/10.3390/coatings11070747>
- [27] H. Yang, X. Guo, G. Wu, W. Ding, N. Birbilis, Electrodeposition of chemically and mechanically protective Al-coatings on AZ91D Mg alloy, *Corros. Sci.* 53 (2011) 381–387.
<https://doi.org/10.1016/j.corsci.2010.09.047>
- [28] C. Singh, S. K. Tiwari, R. Singh, Exploring environment friendly nickel electrodeposition on AZ91 magnesium alloy: Effect of prior surface treatments and bath temperature on corrosion behaviour, *Corros. Sci.* 151 (2019) 1–19.
<https://doi.org/10.1016/j.corsci.2019.02.004>
- [29] R. C. Zeng, K. Jiang, S. Q. Li, F. Zhang, H. Z. Cui, E. H. Han, Mechanical and corrosion properties of Al/Ti film on magnesium alloy AZ31B, *Front. Mater. Sci.* 9 (2015) 66–76.
<https://doi.org/10.1007/s11706-015-0272-1>
- [30] W. Jin, G. Wang, Z. Lin, H. Feng, W. Li, X. Peng, A. M. Qasim, P. K. Chu, Corrosion resistance and cytocompatibility of tantalum-surface-functionalized biomedical ZK60 Mg alloy, *Corrosion Science* 114 (2017) 45–56.
<https://doi.org/10.1016/j.corsci.2016.10.021>
- [31] B. Singh, G. Singh, B. S. Sidhu, Analysis of corrosion behaviour and surface properties of plasma-sprayed composite coating of hydroxyapatite-tantalum on biodegradable Mg alloy ZK60, *J. Compos. Mater.* 53 (2019) 2661–2673.
<https://doi.org/10.1177/0021998319839127>
- [32] R. Zeng, W. Dietzel, J. Chen, W. Huang, J. Wang, Corrosion behavior of TiO₂ coating on magnesium alloy AM60 in Hank's solution, In: *Key Engineering Materials*, Trans. Tech. Publications Ltd., 2008, pp. 609–612.
<https://doi.org/10.4028/www.scientific.net/kem.373-374.609>
- [33] Y. Xin, C. Liu, W. Zhang, K. Huo, G. Tang, X. Tian, P. K. Chu, Corrosion resistance of ZrO₂-Zr-coated biodegradable surgical magnesium alloy, *J. Mater. Res.* 23 (2008) 312–319.
<https://doi.org/10.1557/jmr.2008.0040>
- [34] Q. Yang, W. Yuan, X. Liu, Y. Zheng, Z. Cui, X. Yang, H. Pan, S. Wu, Atomic layer deposited ZrO₂ nanofilm on Mg-Sr alloy for enhanced corrosion resistance and biocompatibility, *Acta Biomaterialia* 58 (2017) 515–526.
<https://doi.org/10.1016/j.actbio.2017.06.015>
- [35] Y. H. Zou, J. Wang, L. Y. Cui, R. C. Zeng, Q. Z. Wang, Q. X. Han, J. Qiu, X. B. Chen, D. C. Chen, S. K. Guan, Y. F. Zheng, Corrosion resistance and antibacterial activity of zinc-loaded montmorillonite coatings on biodegradable magnesium alloy AZ31, *Acta Biomaterialia* 98 (2019) 196–214.
<https://doi.org/10.1016/j.actbio.2019.05.069>
- [36] Y. Xin, C. Liu, W. Zhang, J. Jiang, G. Tang, X. Tian, P. K. Chu, Electrochemical behavior Al₂O₃/Al coated surgical AZ91 magnesium alloy in simulated body fluids, *J. Electrochem. Soc.* 155 (2008) 178.
<https://doi.org/10.1149/1.2844433>
- [37] L. Guo, W. Wu, Y. Zhou, F. Zhang, R. Zeng, J. Zeng, Layered double hydroxide coatings on magnesium alloys: A review, *J. Mater. Sci. Technol.* 34 (2018) 1455–1466.
<https://doi.org/10.1016/j.jmst.2018.03.003>
- [38] F. Peng, D. Wang, D. Zhang, B. Yan, H. Cao, Y. Qiao, X. Liu, PEO/Mg-Zn-Al LDH composite coating on Mg alloy as a Zn/Mg ion-release platform with multi-functions: Enhanced corrosion resistance, osteogenic, and antibacterial activities, *ACS Biomater. Sci. Eng.* 12 (2018) 4112–4121.
<https://doi.org/10.1021/acsbiomaterials.8b01184>
- [39] H. Li, F. Peng, D. Wang, Y. Qiao, D. Xu, X. Liu, Layered double hydroxide/poly-dopamine composite coating with surface heparinization on Mg alloys: Improved anticorrosion, endothelialization and hemocompatibility, *Biomater. Sci.* 6 (2018) 1846–1858.
<https://doi.org/10.1039/c8bm00298c>
- [40] L. Y. Cui, X. H. Fang, W. Cao, R. C. Zeng, S. Q. Li, X. B. Chen, Y. H. Zou, S. K. Guan, E. H. Han, In vitro corrosion resistance of a layer-by-layer assembled DNA coating on magnesium alloy, *Applied Surface Science* 457 (2018) 49–58.
<https://doi.org/10.1016/j.apsusc.2018.06.240>
- [41] L. Y. Cui, H. P. Liu, K. Xue, W. L. Zhang, R. C. Zeng, S. Q. Li, D. K. Xi, E. H. Han, S. K. Guan, In vitro corrosion and antibacterial performance of micro-arc oxidation coating on AZ31 magnesium alloy: Effects of tannic acid, *J. Electrochem. Soc.* 165 (2018) C821–C829.
<https://doi.org/10.1149/2.0941811jes>
- [42] R. C. Zeng, W. C. Qi, Y. W. Song, Q. K. He, H. Z. Cui, E. H. Han, In vitro degradation of MAO/PLA coating on Mg-1.21Li-1.12Ca-1.0Y alloy, *Front. Mater. Sci.* 8 (2014) 343–353.
<https://doi.org/10.1007/s11706-014-0264-6>
- [43] Z. Wei, P. Tian, X. Liu, B. Zhou, In vitro degradation, hemolysis, and cytocompatibility of PEO/PLLA composite coating on biodegradable AZ31 alloy, *J.*

- Biomed. Mater. Res. B Appl. Biomater. 103 (2015) 342–354. <https://doi.org/10.1002/jbm.b.33208>
- [44] R. C. Zeng, L. Y. Cui, K. Jiang, R. Liu, B. D. Zhao, Y. F. Zheng, In vitro corrosion and cytocompatibility of a microarc oxidation coating and poly(l-lactic acid) composite coating on Mg-1Li-1Ca alloy for orthopedic implants, ACS Appl. Mater. Interfaces 8 (2016) 10014–10028. <https://doi.org/10.1021/acsami.6b00527>
- [45] C. Yu, L. Y. Cui, Y. F. Zhou, Z. Z. Han, X. B. Chen, R. C. Zeng, Y. H. Zou, S. Q. Li, F. Zhang, E. H. Han, S. K. Guan, Self-degradation of micro-arc oxidation/chitosan composite coating on Mg-4Li-1Ca alloy, Surface and Coatings Technology 344 (2018) 1–11. <https://doi.org/10.1016/j.surfcoat.2018.03.007>
- [46] K. Bai, Y. Zhang, Z. Fu, C. Zhang, X. Cui, E. Meng, S. Guan, J. Hu, Fabrication of chitosan/magnesium phosphate composite coating and the in vitro degradation properties of coated magnesium alloy, Materials Letters 73 (2012) 59–61. <https://doi.org/10.1016/j.matlet.2011.12.102>
- [47] H. Ahmadi, R. Ghamsarizade, V. Haddadi-Asl, H. Eivaz Mohammadlo, B. Ramezanzadeh, Designing a novel bio-compatible hydroxyapatite (HA)/hydroxyquinoline (8-HQ)-inbuilt polyvinylalcohol (PVA) composite coatings on Mg AZ31 implants via electrospinning and immersion protocols: Smart anti-corrosion and anti-bacterial properties reinforcements, Journal of Industrial and Engineering Chemistry 116 (2022) 556–571. <https://doi.org/10.1016/j.jiec.2022.09.043>
- [48] I. M. Jipa, A. Stoica, M. Stroescu, L. M. Dobre, T. Dobre, S. Jinga, C. Tardei, Potassium sorbate release from poly(vinyl alcohol)-bacterial cellulose films, Chemical Papers 66 (2012) 138–143. <https://doi.org/10.2478/s11696-011-0068-4>
- [49] A. S. Al-Gorair, H. Hawsawi, A. Fawzy, M. Sobhi, Ahmed Alharbi, R. S. Abdel Hameed, S. Abd El Wanees, M. Abdallah, Evaluation of the anticorrosion and adsorption properties of polyethylene glycol and polyvinyl alcohol for corrosion of iron in 1.0 M NaCl solution, Int. J. Electrochem. Sci. 16 (2021) 1–19. <https://doi.org/10.20964/2021.11.03>
- [50] H. Khatun, M. Rahman, S. Mahmud, M. Rahaman, O. Ali, Y. Ali, S. Islam, Synthesis and characterization of biocompatible hybrid coating on WE54 Mg alloy for implant applications, Results in Engineering 21 (2024) 101784. <https://doi.org/10.1016/j.rineng.2024.101784>
- [51] N. Ahuja, N. S. Grewal, K. Kumar, U. Batra, Investigating in-vitro degradation, fatigue behavior, and fracture toughness of electrical discharge-processed Mg alloys for biodegradable implant applications, International Journal of Lightweight Materials and Manufacture 7 (2024) 293–307. <https://doi.org/10.1016/j.ijlmm.2023.11.001>
- [52] F. Delogu, G. Gorrasi, A. Sorrentino, Fabrication of polymer nanocomposites via ball milling: Present status and future perspectives, Progress in Materials Science 86 (2017) 75–126. <https://doi.org/10.1016/j.pmatsci.2017.01.003>
- [53] P. Baláž, M. Achimovičová, M. Baláž, P. Billik, Z. Cherkezova-Zheleva, J. Manuel Criado, F. Delogu, E. Dutková, E. Gaffet, F. J. Gotor, R. Kumar, I. Mitov, T. Rojác, M. Senna, A. Streletskii, K. Wiczorek-Ciurowa, Hallmarks of mechanochemistry: From nanoparticles to technology, Chem. Soc. Rev. 42 (2013) 7571–7637. <https://doi.org/10.1039/c3cs35468g>
- [54] G. Walker (Ed.), Solid state hydrogen storage: materials and chemistry. Woodhead Pub., 2008. Hardback ISBN: 9781845692704, eBook ISBN: 9781845694944.
- [55] T. Kokubo, H. Takadama, How useful is SBF in predicting in vivo bone bioactivity?, Biomaterials 27 (2006) 2907–2915. <https://doi.org/10.1016/j.biomaterials.2006.01.017>
- [56] A. S. Asran, S. Henning, G. H. Michler, Polyvinyl alcohol-collagen-hydroxyapatite biocomposite nanofibrous scaffold: Mimicking the key features of natural bone at the nanoscale level, Polymer (Guildf) 51 (2010) 868–876. <https://doi.org/10.1016/j.polymer.2009.12.046>
- [57] I. M. Jipa, A. Stoica, M. Stroescu, L. M. Dobre, T. Dobre, S. Jinga, C. Tardei, Potassium sorbate release from poly(vinyl alcohol)-bacterial cellulose films, Chemical Papers 66 (2012) 138–143. <https://doi.org/10.2478/s11696-011-0068-4>
- [58] C. Tsiptsias, D. Fardis, X. Ntampou, I. Tsivintzelis, C. Panayiotou, Thermal behavior of poly(vinyl alcohol) in the form of physically crosslinked film, Polymers (Basel) 15 (2023) 1843. <https://doi.org/10.3390/polym15081843>
- [59] G. Balakrishnan, R. Velavan, K. Mujasam Batoo, E. H. Raslan, Microstructure, optical and photocatalytic properties of MgO nanoparticles, Results Phys. 16 (2020) 103013. <https://doi.org/10.1016/j.rinp.2020.103013>
- [60] T. D. Munusamy, S. Sarmin, H. R. Ong, W. T. Gan, C. S. Hong, M. M. R. Khan, Catalytic performance and antimicrobial activity of Mg(OH)₂/MgO colloidal nanoparticles in alkyd resin nanocomposite derived from palm oil, Polymer Bulletin 77 (2020) 4571–4586. <https://doi.org/10.1007/s00289-019-02993-8>
- [61] Y. Yahşi, R. Ipek, Effects of mechanical milling and fast sintering on Mg powders: Microstructural analysis and mechanical properties, Gazi University Journal of Science 37 (2024) 1436–1449. <https://doi.org/10.35378/guis.1372318>